REFERENCES

[1] G. Schaller, "Directivity improvement of microstrip $\lambda/4$-directional couplers," *Arch. Elek. Übertragung*, vol. 26, pp. 508–509, 1972.
[2] D. C. Richard, "Thick film MIC components in the range 10–20 GHz," in *Proc. 1976 European Microwave Conf.* (Rome, Italy, 1976), pp. 687–691.
[3] C. Buntschuh, "High directivity microstrip couplers using dielectric overlays," in *IEEE MTT Symp. Digest*, 1975, p. 125.
[4] F. C. de Ronde, "A new class of microstrip directional couplers," in *Proc. 1970 IEEE Int. Microwave Symp.* (May 1970), pp. 184–186.
[5] J. A. Garcia, "A wide-band quadrature hybrid coupler," *IEEE Trans. Microwave Theory Tech.*, vol. MTT-19, pp. 660–661, July 1971.
[6] B. Schiek, "Hybrid branchline couplers—A useful new class of directional couplers," *IEEE Trans. Microwave Theory Tech.*, vol. MTT-22, pp. 864–869, Oct. 1974.

The Design of Interdigitated Couplers for MIC Applications

VITTORIO RIZZOLI AND ALESSANDRO LIPPARINI

Abstract—**A straightforward design procedure for microstripline interdigitated directional couplers is outlined. Based on exact, closed-form equations for coupler analysis, a design chart is developed allowing the geometry of the cross section to be found, starting from a prescribed coupling and given bounds on directivity and VSWR. A further chart yields the length of the coupled section once the center-band frequency has been fixed. In this way, a complete picture of coupler performance is made available to the designer so that the necessary tradeoffs between coupling, directivity, and impedance match can be predicted and understood. The accuracy of the design procedure is also discussed in relation with the most important parasitics affecting coupler behavior, such as launching-discontinuity effects and bonding-wire reactances.**

I. INTRODUCTION

MICROSTRIP interdigitated topologies represent the most effective and popular means of realizing wide-band–tight-coupling devices—such as octave-band quadrature hybrids—for MIC applications. Since the original works by Lange [1] and Waugh and La Combe [2], who described empirically tailored devices, considerable attention has been devoted in the literature to the problem of predicting the behavior of such components on a quantitative basis [3]–[7], and several design procedures have been proposed.

However, a number of aspects of the analysis and design problem concerning this kind of device have not been covered so far. Among these are: a clear explanation of the physical mechanism giving rise to the high directivity of the interdigitated coupler; a detailed analysis of the effects of parasitics (such as due to launching discontinuities and bonding wires) on coupler performance; and the development of a design procedure allowing directivity (besides coupling and impedance level) to be predicted and possibly optimized for any prescribed coupling.

Manuscript received March 11, 1977; revised May 26, 1977. This work was supported by the Italian National Research Council. Part of this work was presented at the 6th European Microwave Conference, Rome, Italy, September 1976.

The authors are with the Istituto di Elettronica, University of Bologna, Villa Griffone, Pontecchio Marconi, Bologna, Italy.

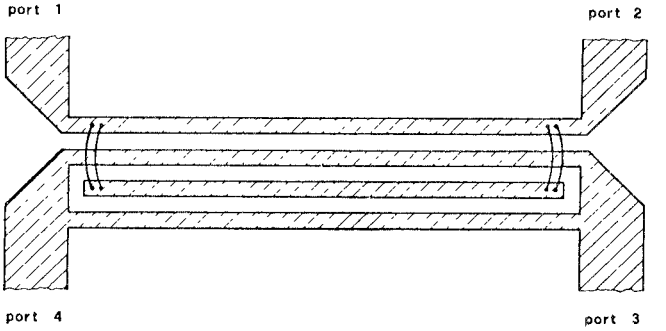

Fig. 1. Schematic of "unfolded" interdigitated couplers.

In order to attempt an answer to the previous questions, an exact analysis of coupler operation is carried out in the present paper. The approach used relies upon the even- and odd-network concept [8], allowing simple, explicit formulas for coupler analysis to be derived. The latter are then used to generate frequency-independent design charts yielding the coupler geometry for prescribed coupling and directivity. The same approach provides a simple means of accounting for the most important parasitic effects, including launching discontinuities and losses. These effects are shown to be responsible for the discrepancies between theoretical and experimental results. Finally, some physical insight into the problem of coupler directivity is provided.

II. COUPLER ANALYSIS AND DESIGN

A microstrip interdigitated coupler in the so-called "unfolded" [2] configuration is shown schematically in Fig. 1. The device basically consists of a length of an axially uniform four-microstrip system whose alternate conductors are short circuited at both ends of the coupled section to yield the interdigitated topology. The strips are assumed to be equal and equally spaced since this is the most commonly

0018-9480/78/0100-0007$00.75

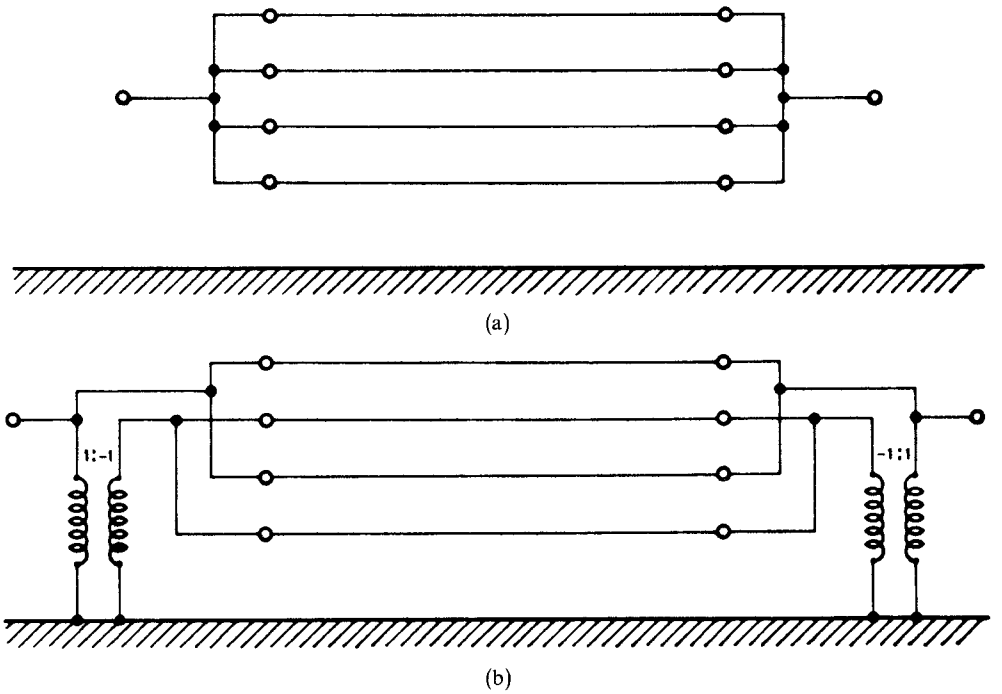

Fig. 2. (a) Schematic of even network. (b) Schematic of odd network

encountered configuration. Thus the only two design parameters are strip width and spacing, once substrate thickness and permittivity have been fixed.

As a first approach to the problem, the device is modeled as a loss-free, inhomogeneous, quasi-TEM four-wire line, and any parasitic effects are neglected. If this is the case, the voltage and current distributions on the strips associated with the independent modes of propagation are defined by the following matrices (propagation factors of the form $\exp(-j\omega z/v_{pi})$ are understood):

$$V = \begin{bmatrix} 1 & 1 & k_3 & k_4 \\ -k_1 & k_2 & -1 & 1 \\ k_1 & k_2 & -1 & -1 \\ -1 & 1 & k_3 & -k_4 \end{bmatrix} \tag{1}$$

and

$$I = \begin{bmatrix} 1 & 1 & k_2 & k_1 \\ -k_4 & k_3 & -1 & 1 \\ k_4 & k_3 & -1 & -1 \\ -1 & 1 & k_2 & -k_1 \end{bmatrix} \cdot U \tag{2}$$

where U is a diagonal matrix,

$$U = (u_1, u_2, u_3, u_4). \tag{3}$$

The k's and u's and the phase velocities v_{pi} may be computed by the explicit formulas reported in the Appendix, starting from the capacitance matrices of the line. The latter can be related to strip width (w) and spacing (s) via conventional multiwire-line analysis [9].

From (1) and (2) the network is seen to support two even and two odd modes with respect to the axial plane of symmetry. Thus despite the interdigitated topology, one can take advantage of the concepts of even and odd networks [8] and reduce the analysis problem to one of two uncoupled two-port networks, having the simple topologies shown in Fig. 2.

In each case, only two of the normal modes are fed, so that the analysis is easily carried out in closed form. If the ports are numbered as in Fig. 1 and a common reference impedance R is chosen, then the following expressions are obtained for the scattering parameters of the directional coupler:

$$\begin{aligned} s_{11} &= \xi_E + \xi_O - 1 \\ s_{12} &= \delta_E \xi_E + \delta_O \xi_O \\ s_{13} &= \delta_E \xi_E - \delta_O \xi_O \\ s_{14} &= \xi_E - \xi_O. \end{aligned} \tag{4}$$

The even-mode parameters δ_E, ξ_E appearing in (4) are given by

$$\delta_E = \frac{q_2 \csc \theta_2 + q_3 \csc \theta_3}{q_2 \cot \theta_2 + q_3 \cot \theta_3 + j}$$

$$\xi_E = \frac{1}{1 - j[q_2 \cot \theta_2 + q_3 \cot \theta_3 - \delta_E(q_2 \csc \theta_2 + q_3 \csc \theta_3)]} \tag{5}$$

where θ_i is the electrical length of the ith mode and

$$\begin{aligned} q_2 &= Ru_2 \frac{(k_3 + 1)^2}{k_2 k_3 + 1} \\ q_3 &= Ru_3 \frac{(k_2 - 1)^2}{k_2 k_3 + 1}. \end{aligned} \tag{6}$$

To obtain the corresponding odd-mode parameters δ_O, ξ_O, one just replaces the subscripts 2 and 3 by 4 and 1, respectively, in (5) and (6).

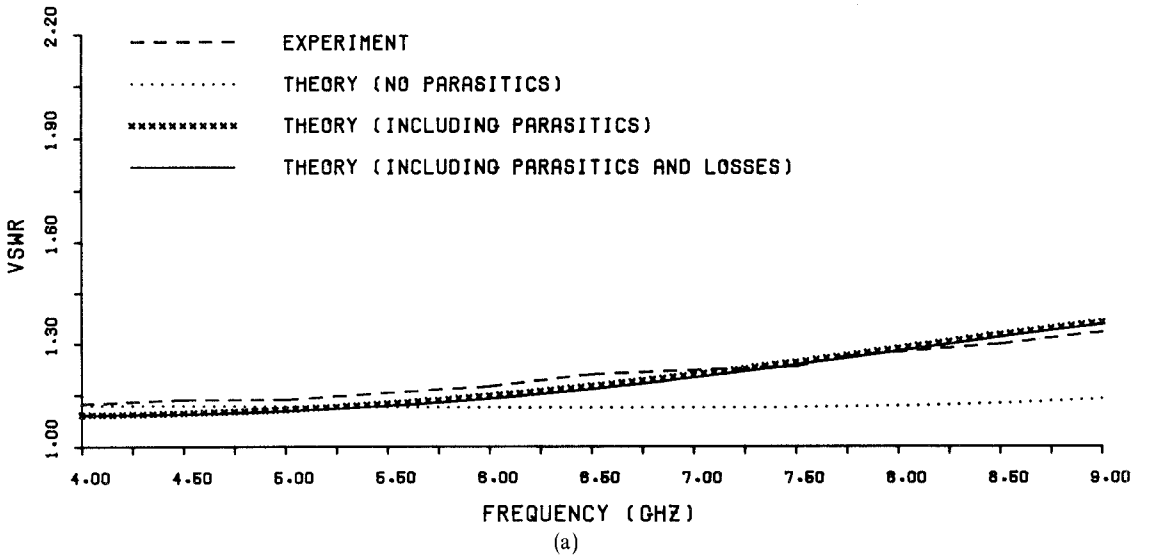

(a)

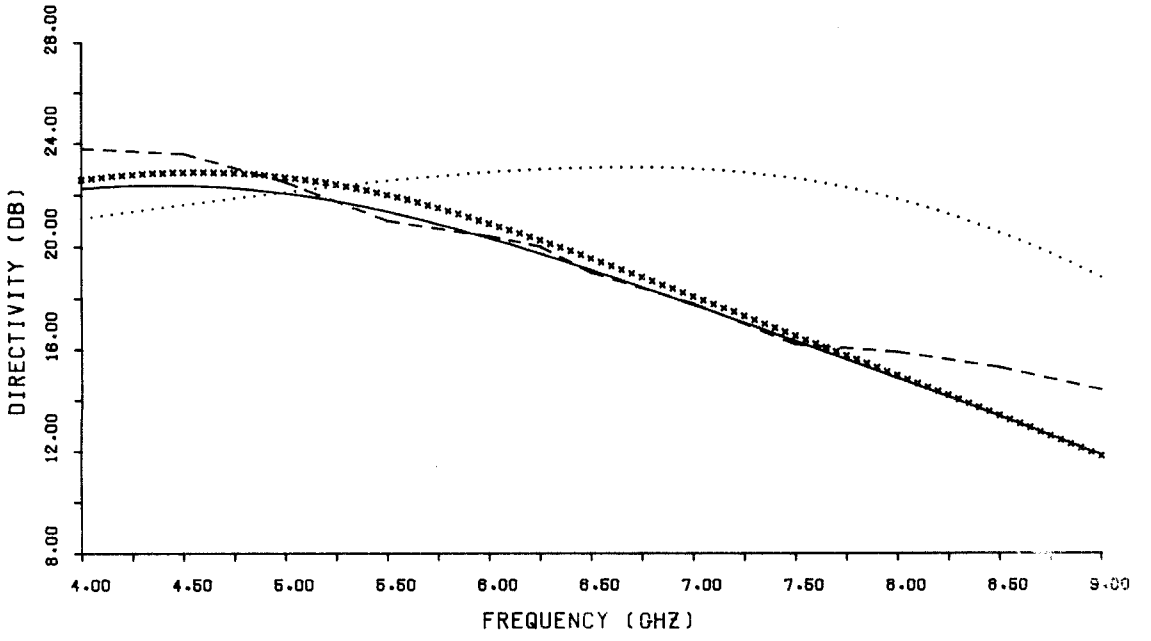

(b)

Fig. 3. Comparison between measured and computed performance of interdigitated couplers.

The validity of these formulas was tested by comparing the computed and measured performances of a practical alumina 3-dB coupler, having $w \simeq 70\ \mu$m, $s \simeq 50\ \mu$m, and a length of the coupled section of about 4.45 mm. The comparison is displayed in Fig. 3, where the main parameters defining coupler performance, that is, input VSWR, directivity, coupling, and insertion loss, are plotted against frequency (by dotted lines). While the agreement is not perfect, it is evident that the behavior of the device, including directivity, can be predicted with practically significant accuracy.

Now let l be the length of the coupled section. In the simple schematization considered so far, the scattering matrix of the coupler depends on frequency only through the product fl appearing in (5). This allows a universal, that is, frequency-independent, design chart to be drawn for any given substrate characteristics. Such a chart for 0.635-mm alumina is presented in Fig. 4 and consists of a number of constant center-band coupling and directivity curves plotted on the w–s plane. To generate these curves a number of grid points were first established in the w–s plane and for each one of these the center-band coupling and directivity were found by seeking the fl value yielding maximum coupling. Then the curves could be sketched by interpolation. Constant VSWR curves can be obtained in a similar way; the one corresponding to an input standing-wave ratio of 1.2 is drawn in Fig. 4 by a thick solid line. The region where VSWR < 1.2 is indicated as well. To complete the design information, in Fig. 5 the center-band fl product is plotted as a function of strip width for different values of coupling. From this figure the length of the coupled section can be readily obtained once the prescribed center-band frequency is given. Thanks to the use of a very efficient variational procedure [9] for capacitance computations and

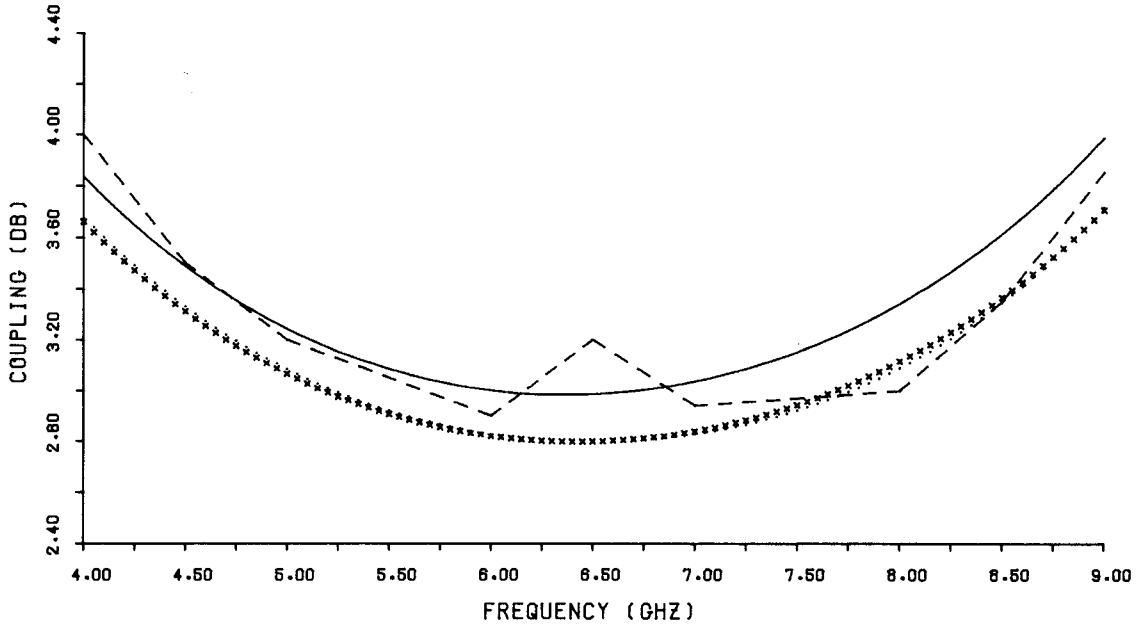

(c)

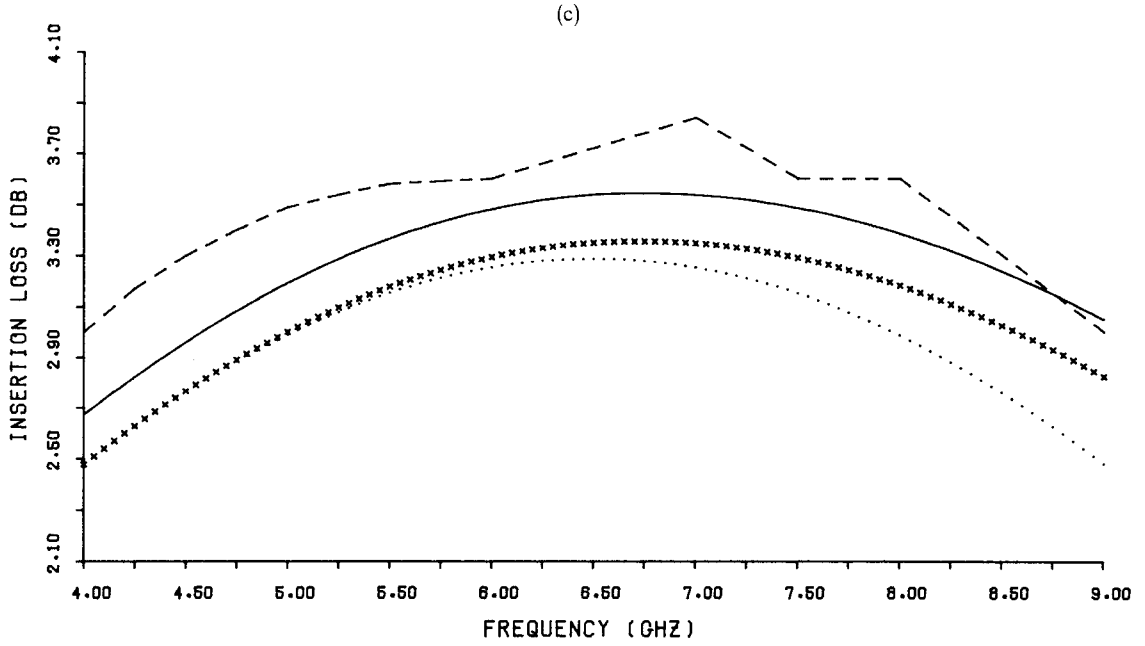

(d)

Fig. 3. (*Continued*).

the explicit formulas (4), it was possible to keep the requirements in computer time within reasonable limits.

From Fig. 4 it is evident that coupling values between 2 and 6 dB with good directivities are well within the reach of present-day technology. It is interesting to observe that coupling essentially depends on strip spacing only, at least in the region where VSWR < 1.2. On the other hand, for any given coupling value (i.e., strip spacing) there exists an optimum choice of strip width, yielding maximum directivity. This optimum point always lies within the region of good input match. Note, anyway, that the performance of the coupler does not depend very critically on the geometrical parameters, which explains the relatively wide spread of different designs for the 3-dB hybrid that have appeared in the literature.

III. Effects of Parasitics

In order to improve the agreement between theory and experiment, particularly to explain the rolloff of directivity and the increase of VSWR with increasing frequency, the analytical model of the coupler should be refined. This can be done by considering additional effects, such as parasitics and losses. Unfortunately, when these are included it is no longer possible to draw frequency-independent design charts such as Fig. 4, since the scattering matrix of the coupler no longer contains frequency in the fl combination only. Thus for a practical design the chart could be best used to find a reasonable starting point for a local optimization to be carried out by a more sophisticated model. In this section the effects of launching discontinuities, bridging connec-

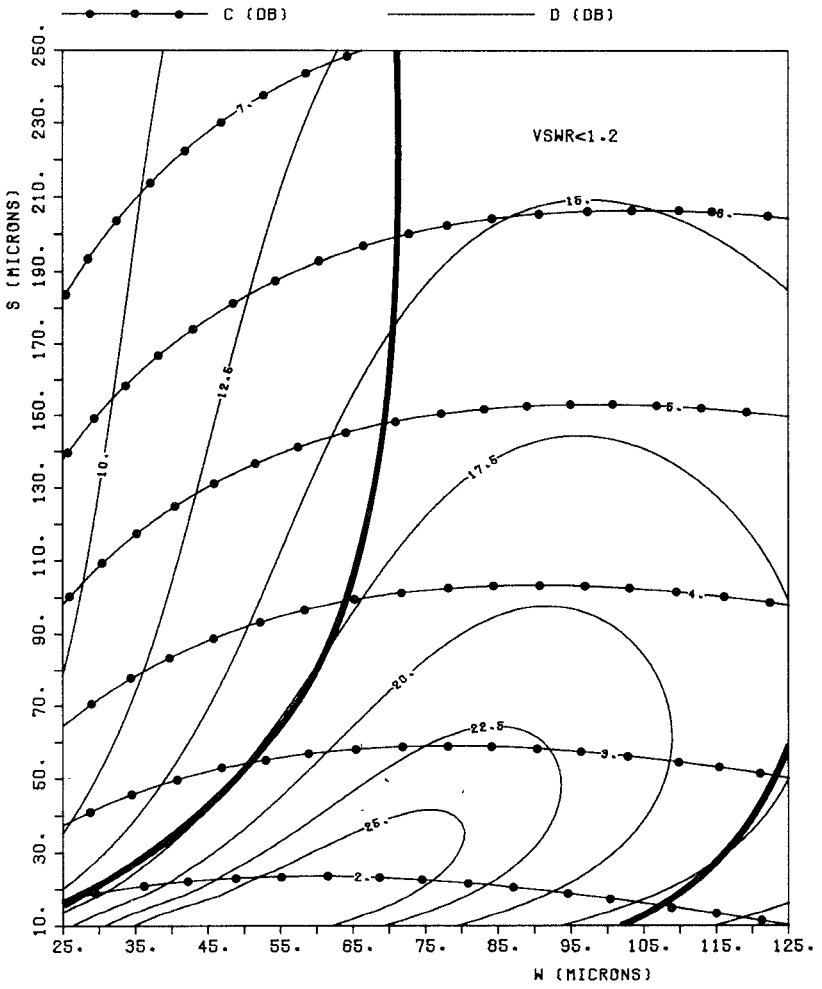

Fig 4 Design chart for alumina interdigitated couplers

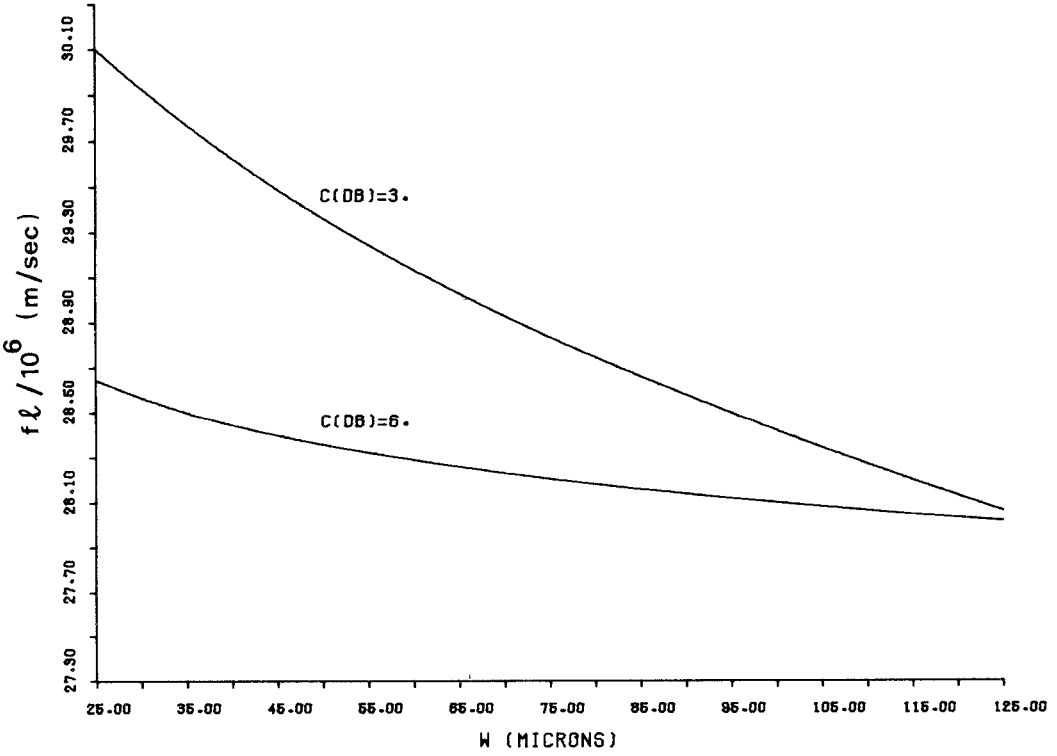

Fig 5 Center-band fl product for alumina interdigitated couplers

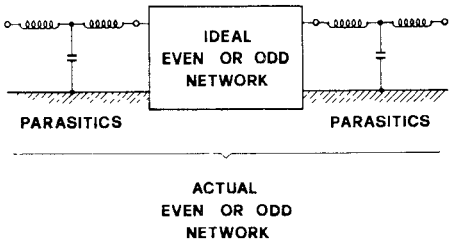

Fig. 6. Circuit model of launching parasitics.

tions, and losses will be discussed and it will be shown that, when these are taken into account, one can achieve a fairly accurate theoretical characterization of coupler behavior.

Junction parasitics are considered first. At both ends of the coupler, discontinuity effects occur at the junction between the very narrow coupled section and the relatively wide 50-Ω line, as schematically illustrated in Fig. 1. Now there is a very simple way these effects can be included in the theoretical picture of the coupler. In fact, consider the even and odd networks: for each one of these, the electrical situation at the ends of the coupled section is much the same as due to an impedance step in a conventional microstrip. Thus launching parasitics can be modeled as lumped *LC* low-pass ladders [10] which are cascade connected to the input and the output ports of each network, as shown in Fig. 6. The values of inductances and capacitances can be computed as in [10], [11]. The predicted performance of the coupler, including launching parasitics, is plotted in Fig. 3 by crossed lines. The figure clearly shows that these effects are mainly responsible for the previously observed discrepancies between theoretical and experimental results.

To account for conductor losses, the general formulation described in [12] can be followed. The four quasi-TEM modes of the four-wire line are separately considered, and for each one the current distributions on the strip surfaces are found by static methods starting from the voltage values given by (1). Then the conductor losses are found for each mode by a first-order perturbation technique. For the 3-dB coupler described in Fig. 3, the following expressions were found for the frequency-dependent attenuation constants of the normal modes, assuming smooth strip conductors:

$$\begin{aligned} \alpha_1 &= 0.1739\sqrt{f} \\ \alpha_2 &= 0.0410\sqrt{f} \\ \alpha_3 &= 0.3124\sqrt{f} \\ \alpha_4 &= 0.4551\sqrt{f} \end{aligned} \tag{7}$$

where all of the α's are in decibels/centimeter and f is in gigahertz. These loss factors are easily introduced into the analytical model of the coupler by changing θ_i in (5) into the complex quantity $(\theta_i - j\alpha_i l)$. The theoretical performance of the coupler with losses included is again plotted in Fig. 3 (solid lines). Only an average discrepancy of about 0.2 dB is observed between the computed and measured insertion loss: this is probably due to conductor roughness, giving rise to an increase in attenuation constants that is unpredictable by computation. Note that losses play a relatively significant role on coupling and insertion loss, while directivity and input VSWR are almost unaffected.

Finally, the effect of bridging connections is considered. To account for these, the bonding wires in Fig. 1 are modeled as lumped inductors instead of short circuits. The shape is assumed to be half-circular and the inductance is computed at a rate of 10 nH/cm [13]. However, when these inductances are not neglected, the formulas (4) are no longer valid and the analysis must be performed by a general-purpose computer program including a facility for multiwire-line characterization [9]. Fig. 7 shows that the effect of imperfect connections on coupling, insertion loss, and input impedance is negligible for all practical purposes. On the other hand, the effect on directivity is more important: for the case considered here it changes by about 1 dB over the whole frequency band. Note that directivity *increases* with respect to the theoretical value as a consequence of nonzero bridging inductances. Thus one is allowed to design the coupler with the assumption of ideal crossovers, since this turns out to be a worst-case design.

IV. Coupler Directivity: Comparison with Two-Wire Couplers

The design chart presented in Fig. 4 shows that 3-dB couplers with directivities well above 22 dB can be obtained by the interdigitated topology. To account for these high values and for the rapid decrease of directivity with decreasing coupling, a few considerations will be developed in the present section about the center-band behavior of the coupler.

In order to simplify the analytical derivations and to obtain simple explicit formulas to work with, let us first assume that the even and odd networks of Fig. 2 can be equivalently represented by two uncoupled transmission-line sections. On a qualitative ground this is not a misleading assumption since the behavior of the interdigitated coupler and the conventional two-wire one are known to be substantially similar [4], [6]. Thus we may speak in terms of equivalent even- and odd-mode characteristic impedances (Z_E, Z_O) and phase velocities (v_E, v_O). If this is the case, the condition for optimum input match becomes

$$Z_E Z_O = R^2 \tag{8}$$

and the center-band is approximately defined by

$$\begin{aligned} \theta_E &= \frac{\omega l}{v_E} = \frac{\pi}{2} + \delta \\ \theta_O &= \frac{\omega l}{v_O} = \frac{\pi}{2} - \delta \end{aligned} \tag{9}$$

where

$$\delta = \frac{\pi}{2} \cdot \frac{v_O - v_E}{v_O + v_E}. \tag{10}$$

If the coupler is designed so that (8) holds, δ depends only on substrate permittivity and center-band coupling. In Fig. 8, δ

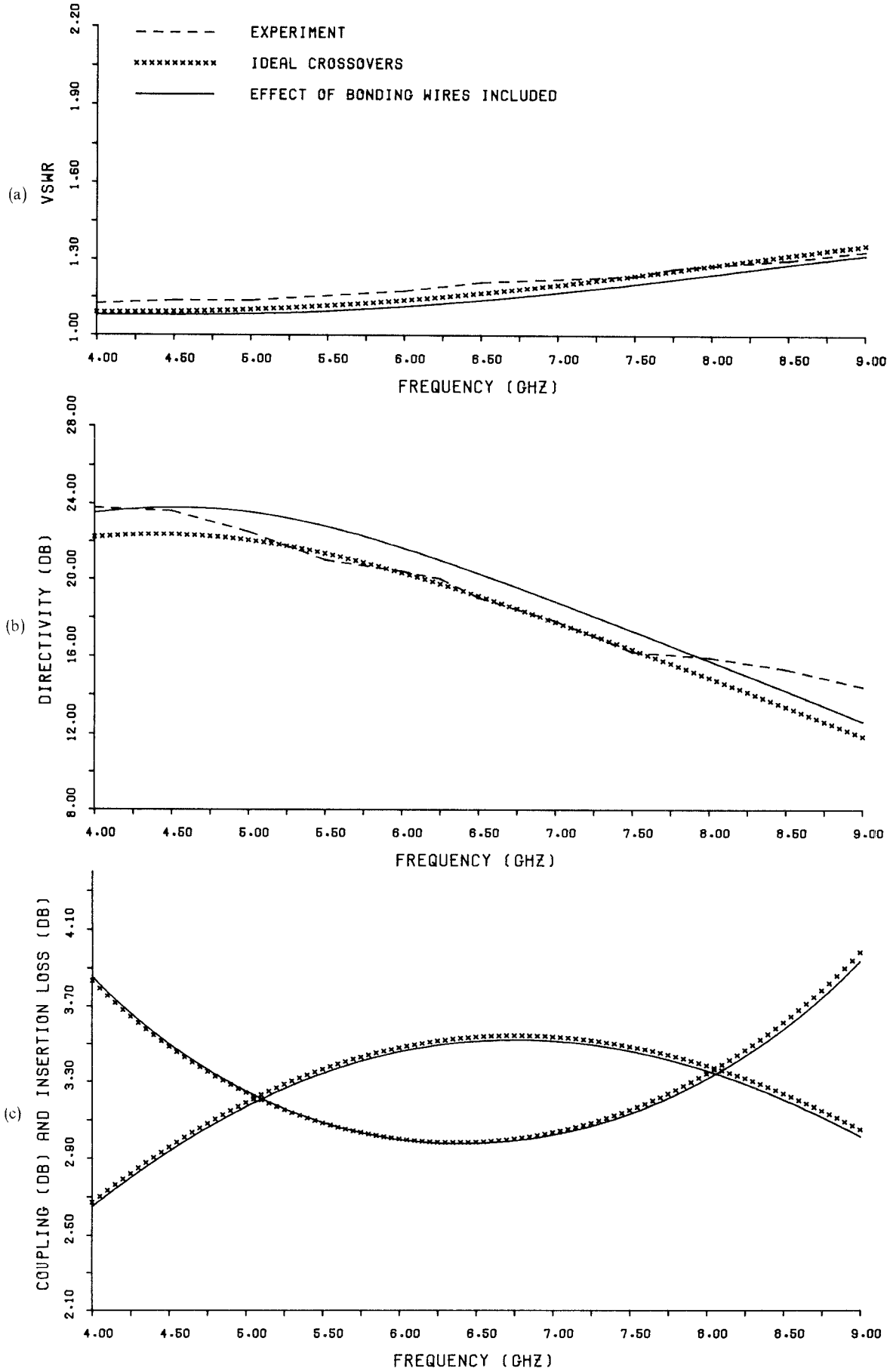

Fig 7 Effects of bonding wires on coupler performance

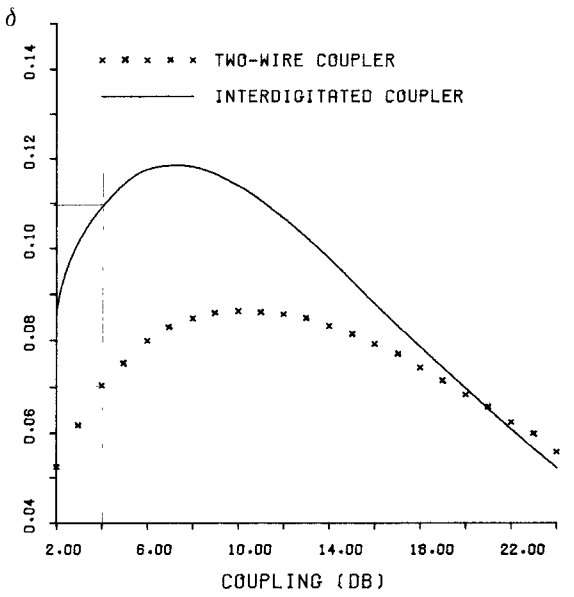

Fig 8 Phase-velocity mismatch versus coupling for conventional and interdigitated microstrip couplers.

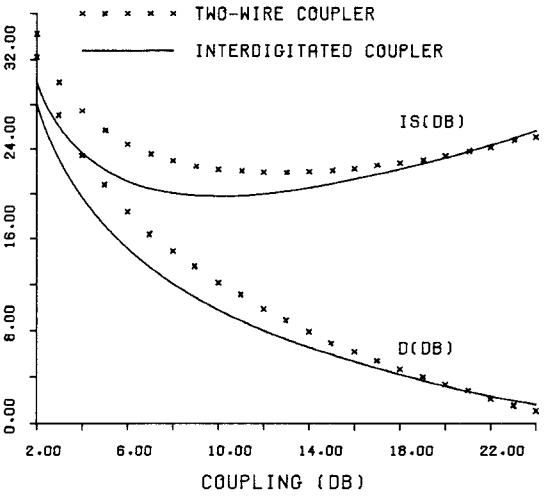

Fig. 9 Center-band directivity and isolation versus coupling for conventional and interdigitated microstrip couplers

is plotted as a function of coupling both for an interdigitated coupler and a conventional two-wire coupler built on 0.635-mm alumina. To draw the curve for the interdigitated coupler, the behavior of the even and odd networks was first exactly computed by (5) and then approximated by simple transmission-line formulas to find v_E and v_O. For the two-wire case, conventional coupled-microstrip analysis was performed.

An interesting fact appearing from Fig. 8 is that no phase-velocity compensation [14] takes place in the interdigitated structure. In fact, the phase-velocity mismatch is larger for this device than for the two-wire one. Note, moreover, that δ is small (< 0.12) and slowly varying with coupling in a wide range of coupling values: the span of δ in the 2–24-dB range is approximately from 0.05 to 0.12.

In the simple approximation being considered, (4) for the scattering parameters of the coupler are replaced by

$$s_{13} = \frac{\sqrt{1-k^2}}{2} \cdot \left[\frac{\csc \theta_E}{\sqrt{1-k^2}\cot\theta_E + j} - \frac{\csc \theta_O}{\sqrt{1-k^2}\cot\theta_O + j} \right]$$

$$s_{14} = j\frac{k}{2}\left[\frac{1}{\sqrt{1-k^2}\cot\theta_E + j} + \frac{1}{\sqrt{1-k^2}\cot\theta_O + j} \right] \quad (11)$$

where

$$k = \frac{Z_E - Z_O}{Z_E + Z_O}. \quad (12)$$

At center-band, thanks to (9) and the fact that $\delta^2 \ll 1$, the previous equations yield

$$|s_{14}| \simeq k$$
$$|s_{13}| \simeq (1-k^2)\delta \quad (13)$$

which can be obtained by neglecting second- (and higher) order terms in δ. The first line of (13) shows that the power transfer to port 4 (the coupled port) is practically the same as in the homogeneous-dielectric case. The second puts into evidence the factors responsible for a finite power transfer to port 3 (the isolated port); that is, the fraction of power that is not coupled, $(1-k^2)$, and the phase-velocity mismatch δ. Now $(1-k^2)$ is increasing with decreasing coupling for small coupling values and then remains practically constant, while δ has the stationary behavior described earlier for couplings between 2 and 24 dB. In any case, both factors have a constant order of magnitude throughout this range. As a consequence, the interdigitated coupler *is essentially a constant-isolation device*, so that directivity is automatically high for tight couplings, but quickly drops as coupling is decreased.

The previous discussion clearly explains the dependence of maximum directivity and isolation on coupling as obtained from the exact formulas (4), which is illustrated in Fig. 9. For comparison, a corresponding plot concerning the microstrip two-wire coupler is presented in the same figure (crossed lines). The interdigitated coupler and the conventional one are seen to behave in a strictly similar way: any important differences are restricted to the geometries of the cross sections required to yield a prescribed performance.

Appendix

In this appendix we report a few formulas allowing the parameters k_i, u_i appearing in (1) and (3) and the TEM-mode velocities of the four-microstrip array to be explicitly related to the elements of the capacitance matrices. Due to symmetry, the capacitance matrix of the line has the form

$$C = \begin{bmatrix} C_{11} & C_{12} & C_{13} & C_{14} \\ C_{12} & C_{22} & C_{23} & C_{13} \\ C_{13} & C_{23} & C_{22} & C_{12} \\ C_{14} & C_{13} & C_{12} & C_{11} \end{bmatrix}. \quad (14)$$

The free-space capacitance matrix has a similar structure and its elements will be denoted by C_{ij0} $(i, j = 1, 2, 3, 4)$.

Since the exact formulas based on (14) are cumbersome, only a simplified version based on the assumption $C_{13} = C_{14} = 0$ will be reported here. The latter may be used to replace the former in all practical cases without significant loss of accuracy.

The expressions for the k's are as follows:

$$k_1 = \frac{-a + \sqrt{a^2 - 4ce}}{2c} \qquad k_4 = -\frac{c}{e}k_1$$
$$k_2 = \frac{-b + \sqrt{b^2 - 4de}}{2d} \qquad k_3 = -\frac{d}{e}k_2 \tag{15}$$

where

$$a = C_{11}(C_{220} - C_{230}) - C_{110}(C_{22} - C_{23})$$
$$b = C_{11}(C_{220} + C_{230}) - C_{110}(C_{22} + C_{23})$$
$$c = C_{120}(C_{22} - C_{23}) - C_{12}(C_{220} - C_{230})$$
$$d = C_{120}(C_{22} + C_{23}) - C_{12}(C_{220} + C_{230})$$
$$e = C_{12}C_{110} - C_{11}C_{120}. \tag{16}$$

The TEM-mode phase velocities are given by

$$v_{pi} = \frac{v_0}{\sqrt{\lambda_i}} \qquad (i = 1, 2, 3, 4) \tag{17}$$

where

$$\lambda_1 = hg\left|i + m - e\left(\frac{1}{k_1} + k_4\right)\right|$$
$$\lambda_2 = hf\left|l + m + e\left(\frac{1}{k_2} + k_3\right)\right|$$
$$\lambda_3 = hf\left|l + m - e\left(\frac{1}{k_2} + k_3\right)\right|$$
$$\lambda_4 = hg\left|i + m + e\left(\frac{1}{k_1} + k_4\right)\right| \tag{18}$$

and v_0 is the velocity of light *in vacuo*. In (18) we have

$$f = C_{110}(C_{220} - C_{230}) - C_{120}^2$$
$$g = C_{110}(C_{220} + C_{230}) - C_{120}^2$$
$$1/h = 2[C_{110}^2(C_{220}^2 - C_{230}^2) - 2C_{110}C_{120}^2C_{220} + C_{120}^4]$$
$$i = C_{110}(C_{22} - C_{23}) + C_{11}(C_{220} - C_{230})$$
$$l = C_{110}(C_{22} + C_{23}) + C_{11}(C_{220} + C_{230})$$
$$m = -2C_{12}C_{120}. \tag{19}$$

Finally, the u's may be expressed as

$$u_1 = v_{p1}(C_{11} - k_1C_{12})$$
$$u_2 = v_{p2}(C_{11} + k_2C_{12})$$
$$u_3 = v_{p3}(C_{22} + C_{23} - k_3C_{12})$$
$$u_4 = v_{p4}(C_{22} - C_{23} + k_4C_{12}). \tag{20}$$

References

[1] J. Lange, "Interdigitated stripline quadrature hybrid," *IEEE Trans. Microwave Theory Tech.*, vol MTT-17, pp. 1150–1151, Dec 1969

[2] R Waugh and D. La Combe, "Unfolding the Lange coupler," *IEEE Trans. Microwave Theory Tech.*, vol. MTT-20, pp. 777–779, Nov 1972

[3] W. P. Ou, "Design equations for an interdigitated directional coupler," *IEEE Trans Microwave Theory Tech.*, vol MTT-23, pp 253–255, Feb 1975

[4] V. Rizzoli, "Stripline interdigitated couplers: Analysis and design considerations," *Electron. Lett.*, vol. 11, pp. 392–393, Aug. 1975.

[5] J. A. G Malherbe, "Interdigital directional couplers with an odd or even number of lines and unequal characteristic impedances," *Electron Lett.*, vol. 12, pp. 464–465, Sept. 1976.

[6] S J Hewitt and R. S. Pengelly, "Design data for interdigital directional couplers," *Electron. Lett.*, vol. 12, pp. 86–87, Feb. 1976

[7] D. D. Paolino, "Design more accurate interdigitated couplers," *Microwaves*, pp. 34–38, May 1976.

[8] J Reed and G. J Wheeler, "A method of analysis of symmetrical four-port networks," *IRE Trans. Microwave Theory Tech.*, vol. MTT-4, pp. 246–252, Oct. 1956

[9] V. Rizzoli, "The calculation of scattering parameters for coupled microstrip arrays of any cross section," *Alta Freq.*, vol. XLII, pp. 191–199, Apr. 1973.

[10] A F. Thomson and A. Gopinath, "Calculation of microstrip discontinuity inductances," *IEEE Trans. Microwave Theory Tech*, vol. MTT-23, pp. 648–655, Aug 1975.

[11] P. Benedeck and P. Silvester, "Equivalent capacitances for microstrip gaps and steps," *IEEE Trans Microwave Theory Tech.*, vol. MTT-20, pp. 729–733, Nov. 1972

[12] V Rizzoli, "Losses in microstrip arrays," *Alta Freq.*, vol. XLIV, pp. 86–94, Feb. 1975

[13] L. Young and H. Sobol, Eds., *Advances in Microwaves*, vol. 8. New York: Academic, 1974, p 151.

[14] J. E. Miley, "Looking for a 3 to 8 dB microstrip coupler?," *Microwaves*, pp. 58–62, Mar. 1974.